

GSC LOSS: A GAUSSIAN SCORE CALIBRATING LOSS FOR DEEP LEARNING

A PREPRINT

 **Qingsong Zhao**

Tongji University, China
qingsongzhao@tongji.edu.cn

 **Shuguang Dou**

Tongji University, China
2010504@tongji.edu.cn

 **Xiaopeng Ji**

Zhejiang University, China
xp.ji@cad.zju.edu.cn

 **Xinyang Jiang**

Microsoft Research Asia
xinyangjiang@microsoft.com

 **Cairong Zhao** ✉

Tongji University, China
zhaocairong@tongji.edu.cn

 **Yin Wang** ✉

Tongji University, China
yinw@tongji.edu.cn

March 3, 2022

ABSTRACT

Cross entropy (CE) loss integrated with softmax is an orthodox component in most classification-based frameworks, but it fails to obtain an accurate probability distribution of predicted scores that is critical for further decision-making of poor-classified samples. The prediction score calibration provides a solution to learn the distribution of predicted scores which can explicitly make the model obtain a discriminative representation. Considering the entropy function can be utilized to measure the uncertainty of predicted scores. But, the gradient variation of it is not in line with the expectations of model optimization. To this end, we proposed a general Gaussian Score Calibrating (GSC) loss to calibrate the predicted scores produced by the deep neural networks (DNN). Extensive experiments on over 10 benchmark datasets demonstrate that the proposed GSC loss can yield consistent and significant performance boosts in a variety of visual tasks. Notably, our label-independent GSC loss can be embedded into common improved methods based on the CE loss easily.

Keywords Cross Entropy · Gaussian · Score Calibrating

1 Introduction

With the increasingly more complex data, traditional classification models are insufficient to produce a reliable proposal with a discriminative score. Although a large margin could be obtained by the hard encoding like one-hot, the tuned model fails to be generalized to unknown data due to overfitting. Increasing researchers Hinton et al. [2012], Goodfellow et al. [2013a] have paid attention to the design of a definable regularization approach to improve the generalization ability of the unseen validation set.

Especially, Szegedy et al. [2016] introduced label smoothing (LS) which is a mechanism to regularize the classifier layer by taking an average between the hard labels. Plenty of models have incorporated LS into training procedures ever since Zoph et al. [2018]. However, the non-target categories were dominated by fixed uniform probability, which would trail the capability of LS. Based on LS, Zhang et al. [2021] proposed an Online Label Smoothing (OLS) strategy, which generates soft labels based on the statistics of the model prediction for the target category.

The CE loss portrays the distance between the Softmax output (prediction distribution) and the desired output (label probability distribution), that is, the smaller the value of CE, the closer the two probability distributions are, i.e., maximum likelihood estimation. As shown in Fig.1 (b) and (c), both LS and OLS focus on the reconstruction of distribution of labels. They neglect the distribution of prediction scores, by contrast, this paper proposes a GSC loss to calibrate the distribution of prediction scores for regularizing a DNN. Our method focuses only on the predicted scores

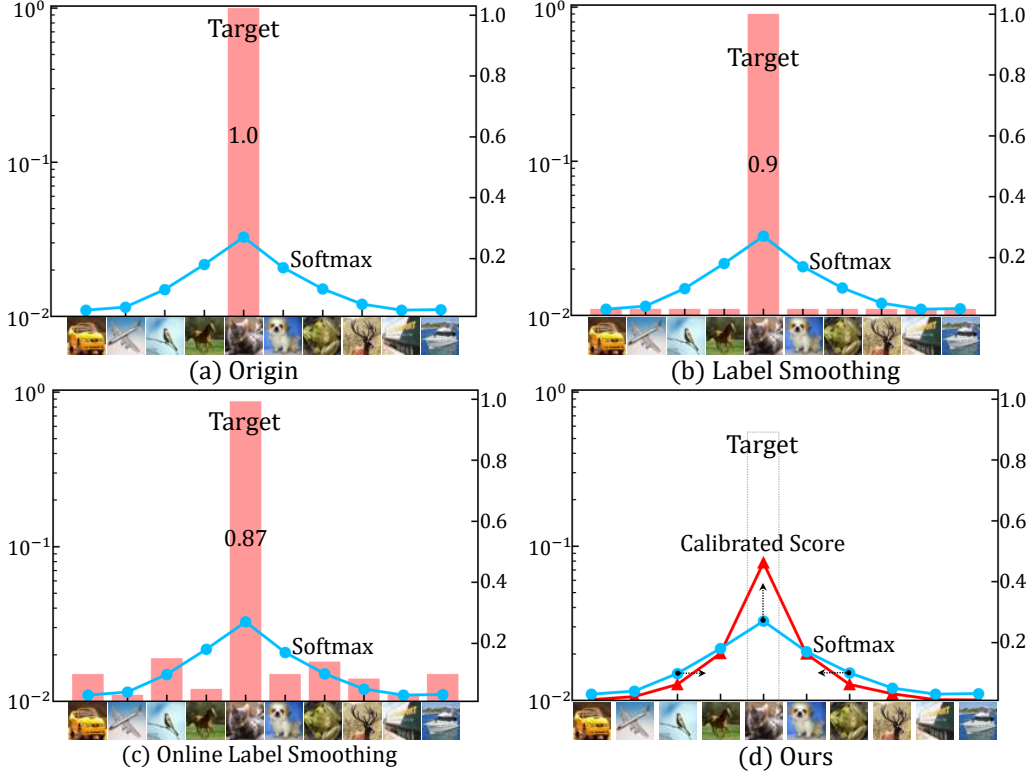


Figure 1: Different kinds of label distributions (Left axis), and prediction distributions (Right axis) on CIFAR-10. (a) A hard label is given for training, this training strategy is actually maximum likelihood estimation (MLE). (b) Soft labels are made by LS for training, this strategy is to make the predicted scores distribution conform to the smoothed label probability distribution. (c) Soft labels are generated by OLS for training, same strategy as (b). (d) Any label is fine, our method is to calibrate the distribution of the predicted scores directly based on the entropy function.

S , hence it has two features: 1) GSC loss can be easily embedded into such soft label based methods as LS, OLS, etc. 2) GSC loss does not depend on labels, which makes it naturally adapted to some unsupervised learning framework.

As illustrated in Fig.1 (d), formulated GSC loss can yield additional controllable penalties on the S to drive the classifier to learn non-overfitting yet discriminative features. Our claims can be verified by Fig.2, compared to such existing baselines as CE loss, focal loss, LS and Entropy loss, the better features could be obtained by the proposed GSC loss. We also use the Expected Calibration Error (ECE) Guo et al. [2017] to measure the calibration ability of those methods, see the ECE values of Fig.2. Compared to those methods, the proposed GSC also achieves lower ECE values. This indicates GSC can make the distance between the prediction distribution and the label probability distribution smaller, i.e., a better calibration capability. Moreover, adequate analysis and experimental results indicate that the GSC loss can alleviate the issue of overfitting by preventing the training loss from quickly falling near to zero, see Sec. 4.3 for details.

To demonstrate the generalization of the proposed GSC loss, we plug it into typical classification visual tasks including facial emotion recognition, image classification, action recognition, and face verification. Experiments show that the effective benefits of GSC loss can be seen in these baselines. The gains from GSC loss are also complementary to recent CE loss-related methods such as LS, OLS, Arcface Deng et al. [2019] and focal loss. Moreover, GSC loss can be easily utilized in unsupervised learning applications. Our contributions can be summarized as follows:

- We propose a controllable GSC loss to calibrate the Softmax output probability S . Its theoretical motivation (Sec. 3.1) is clarified, and a concise theoretical proof (Sec. 3.3) is given.
- We demonstrate that the proposed GSC loss is general and can exert positive influences over existing classification models.

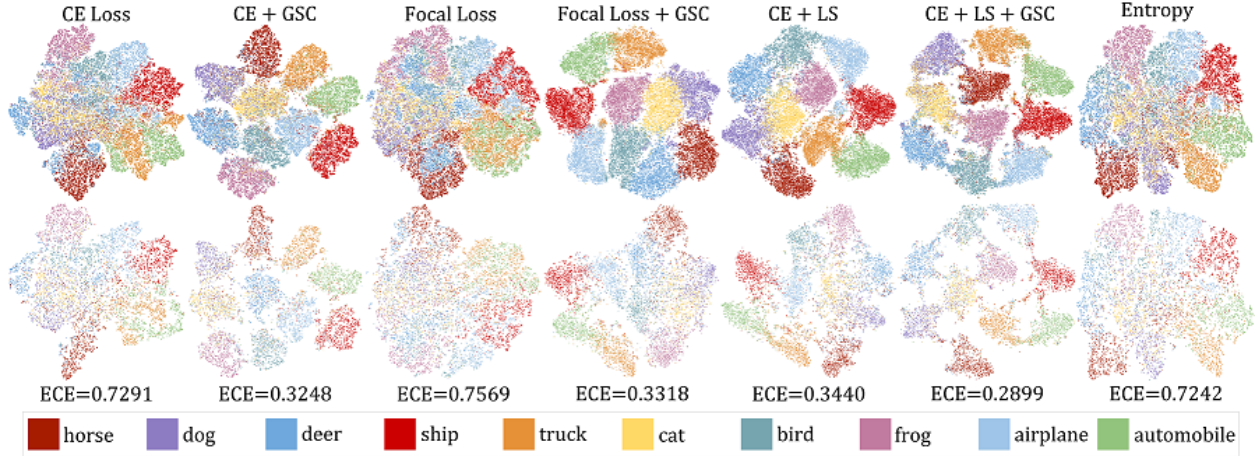


Figure 2: Visualization of classifier layer’s features of Alexnet/CIFAR-10. First row comes from training set, second row from validation set. The first seven columns represent the features extracted from the model which trained by: CE loss, CE w/ GSC loss, focal loss, focal loss w/ GSC loss, CE w/ LS, CE w/ LS w/ GSC loss and CE w/ Entropy loss. The Expected Calibration Error (ECE) on CIFAR-10 validation set was reported. Lower is better.

2 Related Work

Recent works such as contrastive loss Hadsell et al. [2006], triplet loss Schroff et al. [2015], L-Softmax loss Liu et al. [2016], SphereFace Liu et al. [2017], Cosface Wang et al. [2018], Arcface, focal loss and LS etc. have been proposed to enhance the performance of traditional CE loss. In this section, we will briefly overview these methods respectively according to their motivations.

Model Regularization: To alleviate the issue of overfitting, Szegedy et al. [2016] introduced LS. It can improve accuracy by computing cross entropy with a weighted mixture of uniform distribution of targets. In theory, setting the inverse weight for GSC loss can also generate a uniform distribution of classifier scores. LS chooses to discard particularly difficult samples in exchange for gathering simple samples well. In brief, label smoothing should be more friendly to noise samples compared with focal loss. In Müller et al. [2019], Muller *et al.* discussed why and when label smoothing should work, and demonstrated that label smoothing implicitly calibrates learned models. Arguably, the accuracy improvement is not obvious or even decreases if using relatively small networks and face verification tasks with LS.

Discriminatory Feature Learning: To obtain discriminatory features, contrastive loss and triplet loss were introduced gradually. The contrastive loss will require the same class features to be as similar as possible, yet the distance between different class features is larger than a margin. By contrast, the triplet loss requires 3 input samples at a time and maximizes the distance between the anchor and a negative sample. But they all require a carefully designed pair selection procedure. Differently, the L-Softmax loss was proposed in a novel view on the cosine similarity for large-scale face recognition. Inspired by this line, Arcface was introduced to obtain discriminative features. Despite the similarity between ArcFace and previous works, it has a better geometric attribute. But all those methods will increase additional model parameters of W compared with the original softmax function. Meanwhile, to prevent embedding models from learning noisy representations, Shi *et al.* proposed Probabilistic Face Embeddings (PFEs) Shi and Jain [2019]. However, it needs additional calculations to estimate a distribution in the latent space. Moreover, Arcface does not converge well with the PFEs. In contrast to those methods, GSC loss can be embedded into them easily without adding more cost.

Imbalanced Classification: To eliminate the extreme foreground-background class imbalance, effective online hard example mining (OHEM) Shrivastava et al. [2016] was proposed by sampling hard examples during training a network. In contrast, focal loss naturally handles the class imbalance, and efficiently trains on all examples without sampling and without easy negatives. But, the problem is that the model needs to pay excessive attention to difficult samples. Even if the network converged, it may fail to distinguish the outliers. It can also be utilized in standard classification tasks with clean labels. By contrast, GSC loss can inflict additional penalties on ambiguous samples without this problem.

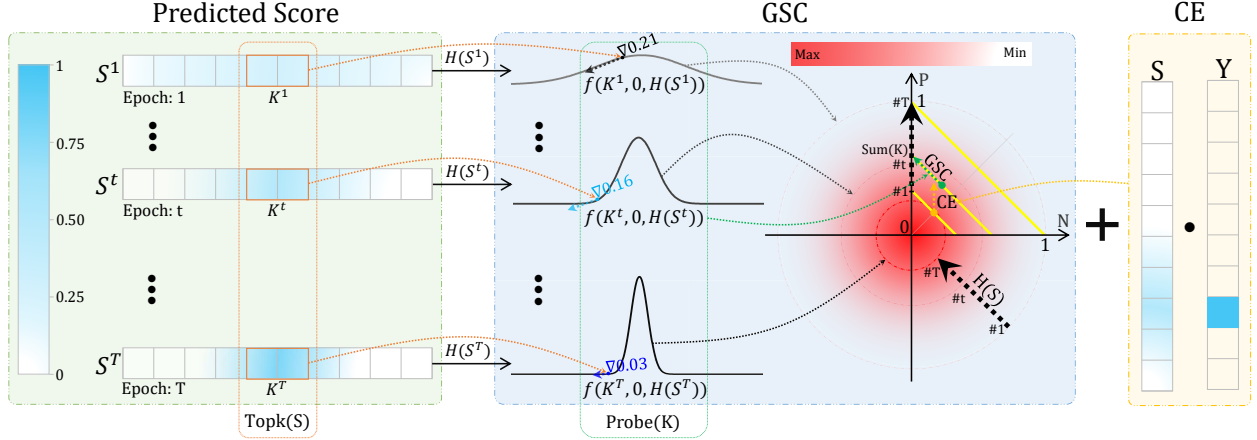


Figure 3: The illustration of training DNN with our GSC loss. First, the images are fed into DNN and softmax to obtain the predicted scores S . The $H(S)$ was computed with the entropy of S , and the $K = \{k_1, k_2, \dots, k_c\}$ was selected by the *Topk* function from S . Then, the $H(s)$ is utilized as an approximate of the variance to construct the GSC loss. The corresponding GSC value is summed with CE loss as the final loss for training.

3 GSC Loss

3.1 Preliminaries

We introduce the GSC loss starting from over-viewing the CE loss for binary classification

$$CE(p, y) = \begin{cases} -\log(p), & \text{if } y = 1 \\ -\log(1 - p), & \text{otherwise,} \end{cases} \quad (1)$$

where $y \in \{0, 1\}$ specifies the target and $p \in [0, 1]$ is the predicted score with label $y = 1$. For clarity, we define p_t :

$$p_t = \begin{cases} p, & \text{Positive, } y = 1 \\ 1 - p, & \text{Negative, } y = 0, \end{cases} \quad (2)$$

and rewrite $CE(p, y) = -\log(p_t)$. Then, the derivative of $CE(p_t)$ is $-1/p_t$. Inspired by the probability distribution estimation technique Nigam et al. [1999], we formulated a discrimination term to give the ambiguous predictions an extra entropy-based punishment. The entropy function $E(p)$ and $E'(p)$ can be written as

$$\begin{cases} E(p) = -[p \log(p) + (1 - p) \log(1 - p)] \\ E'(p) = \log\left(\frac{1 - p}{p}\right). \end{cases} \quad (3)$$

An intuitive explanation was shown in Fig. 4(a), there is a greater learning speed when the error rate (ER) is large. But when the ER is reduced to less than 50%, the backward gradient decreases sharply. Hence, CE loss is not good at improving the discriminative margin among the ambiguous samples Lin et al. [2017]. The initial scores obey a uniform distribution, see Fig. 4(b), as P increases from 0.5 to 0.9, the absolute value of $E'(S)$ rapidly increases from 0 to 2.2. That is not in line with the expectations of model optimization. Notably, the model needs larger backward gradient to enhance the confidence of prediction at the beginning. Later in training, some models produce an over-confidence score, the confidence of model should not be strengthened.

However, the characteristic of $E(S)$ that the maximum value is obtained when the predicted scores are most uncertain could be utilized. Moreover, several comparative experiments between GSC and entropy loss were reported in the Sec. 4.1.

3.2 Definition

Inspired by the characteristic of the above entropy function (First and second derivative of $E(S)$, details see Appendix), we define our GSC loss with regard to the probability density function of one-dimensional Gaussian

$$f(x, \mu, \sigma) = \frac{1}{\sqrt{2\pi}\sigma} \exp\left[-\frac{(x - \mu)^2}{2\sigma^2}\right]. \quad (4)$$

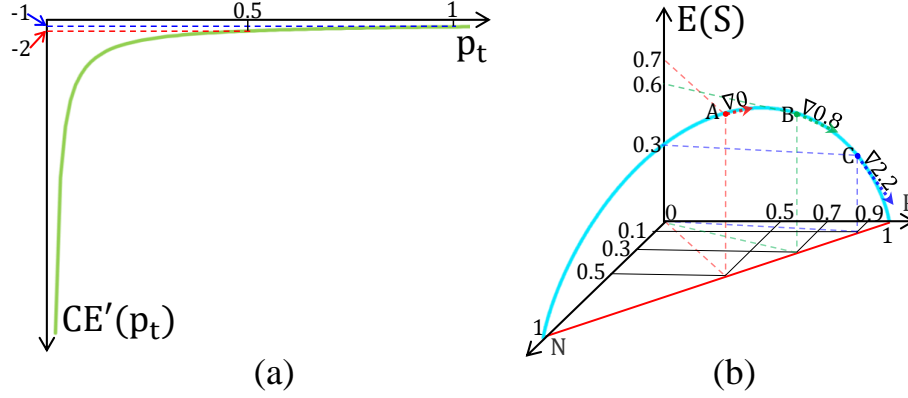


Figure 4: Visualization of the function curves. (a) Function curve of $CE'(p_t)$. (b) Function curve of $E(S)$ in the Eq. 3. P indicates the positive score, N indicates the negative score.

Assume a n -dimensional random variable $S_{n \times 1} = S_i$ ($i \in [1, n]$), and it obeys an n -dimensional Gaussian distribution $f_n(S, \mu, \sigma)$ where all values of the mean vector $\mu_{n \times 1} = \mu_i$ and the covariance vector $\sigma_{n \times 1} = \sigma_i$. The marginal distribution of the multivariate Gaussian distribution is the univariate Gaussian. Thus, $f_n(S, \mu, \sigma)$ can be represented as

$$f_n(S, \mu, \sigma) = \prod_{i=1}^n f(S_i, \mu_i, \sigma_i). \quad (5)$$

Note that μ_i relates to the prediction scores in GSC loss calculation, which are between 0 and 1 across tasks. We chose $\mu_i = 0$ for simplicity, but other small values would probably work too. $\mu_i > 0.5$ can be problematic since it penalizes confident predictions. We denote σ by the entropy of S to measure the uncertainty. This is because entropy is better suited to describe the uncertainty of information than variance, which is descriptive of the uncertainty of information under certain premises Zidek and van Eeden [2003]. A smaller σ means the more certainty of S and the sharper $f_n(S, \mu, \sigma)$, while a larger σ indicates the more uncertainty of S and the more flat distribution curve, see Fig. 3.

In addition, a hypothesis is that one sample is just relevant to a limited number of other categories rather than the whole set. For example, see Fig. 1, ‘cat’ is closer to ‘dog’ and ‘horse’ rather than ‘truck’ or ‘ship’. So we define a function to truncate the predicted score vector by:

$$K = Topk(S, top_c), \quad (6)$$

where S denotes original predicted scores, $top_c \in \mathbb{N}^+ \wedge (0 < top_c \leq n)$ is a hyper-parameter. The $Topk$ sorts S forward, and then outputs the top scores K , see Fig. 3 left. Then, the GSC loss is determined by taking K as a probe on $f_n(K, \mu, \sigma)$, see Fig. 3. Unlike the derivative of entropy function above, Our method is able to maintain a stable backward gradient for the middle and early stages of a DNN training. Later in training, to prevent over-confident predictions, the backward gradient of GSC loss can be quickly reduced to a smaller amount.

Moreover, we provide a mathematical description for multi-class classification. Firstly, with $n \geq 3$ classes, the form of an n -ary entropy function is

$$E(S) = - \sum_{i=1}^n p_i \log(p_i), \quad (7)$$

where $p_i \in S$. The value range of $E(S)$ is $[0, \log(n)]$.

To eliminate the effect of the categories number on the function value, $E(S)$ was rescaled between 0 and 1 by the min-max rescaling method, i.e.,

$$H(S) = \frac{E(S) - 0}{\log(n) - 0}. \quad (8)$$

As a result, the general form of our GSC loss function for multi-class case can be written as

$$L(S, Y) = CE(S, Y) + \gamma f_{top_c}(K, \mu, \sigma), \quad (9)$$

where $\mu_i = 0, \sigma_i = H(S)$. And, if we set $top_c = 2$, it is for the binary classification.

3.3 Interpretation

For clarity, we take a multi-class case with $n = 10$, $top_e = 2$ to explain how the GSC loss works with CE loss. As shown in Fig. 3, here we pay attention to $f(K_1, 0, H(S))$ which is one density function of the marginal distribution of $f_2(K, \mu, \sigma)$ with the different variance value $H(S^t)$, ($t \in [1, T]$).

The weight of a network is usually initialized by normal distribution before the optimization. During the early stage, the predicted scores are a bit smooth i.e., the light grey curve with a large $H(S^1)$, see Fig. 3. At this point, the model need CE loss to correct prediction to the positive direction, also our GSC loss will speed up this process.

As the total loss decline, the output scores will be gradually close to the grey curve with a medium $H(S^t)$. At this point, the model has just learned some loose features and needs to continue to optimize the representation capability. GSC loss will play a more important role in this process than CE.

The final prediction tends to converge with small entropy, i.e., the black curve with a small $H(S)$. At this point, the model have a risk of over-confidence and should be gradually stopped for further optimization.

In addition, there would be two samples that share similar values of the entropy function. For ease of understanding, a top view of $f_2(K, \mu, \sigma)$ was drawn in Fig. 3, P indicates the positive score K_1 , N indicates the negative score K_2 . It is symmetric about $P = 0$ and $N = 0$, and monotonically decreases at $[0, +\infty]$. We assume the predicted score K is constrained by equation $P + N = Sum(K)$. According to the distance formula from a point to the coordinate origin, the formula

$$\underset{(P,N)}{argmax} \quad f_2(K, \mu, \sigma), \quad (10)$$

is equivalent to

$$\underset{(P,N)}{argmin} \quad \sqrt{(P)^2 + (N)^2}. \quad (11)$$

$f_2(K, \mu, \sigma)$ would get the maximum if minimizing its distance to the origin of coordinate, i.e., P is equal to N . It is consistency the precondition that we assume the mean value $\mu = 0$ in Eq. 5. As a result, yielding additional penalties for predicted fuzzy scores while $P \approx N$ is exactly what we expected.

4 Experiments

The goal of this paper is to show that a simple and intuitive loss term gives additional gains on top of the standard CE loss over a variety of vision tasks, even with larger datasets and bigger models. To evaluate the performance of GSC loss, we take into account five typical visual applications including image classification, face verification, facial emotion recognition, action recognition and unsupervised image segmentation. Notably, we do not intend to establish new SOTA for any benchmark. More results are given in the Appendix.

To make a fair comparison, we utilized the same networks in all baseline settings. Note that, we only control the variable of the loss function in all experiments. The other settings, including software and hardware, keep consistent. We also conducted ablation studies to verify the effectiveness of proposed GSC loss on such network models as AlexNet, VGGNet, ResNet-50/101 He et al. [2016] and extended ResNet3D-34 with different depth and structures.

4.1 Image Classification

In the section, we conduct experiments on two general image classification datasets: CIFAR-10 and ImageNet-1K and one fine-grained image classification dataset: Flowers-102 Nilsback and Zisserman [2008].

CIFAR-10: We employ the architecture of AlexNet without batch normalization (BN) layers Krizhevsky [2014] and a Transformer-based model ConvMixer Trockman and Kolter [2022]. CIFAR-10 consists of 60K images in 10 classes, with 6K images per class. We employ the commonly used protocols with the data augmentation Lee et al. [2015]. We compared our GSC loss with those common methods on CIFAR10. In CE loss based methods such as entropy loss, focal loss, and LS, proposed GSC loss obtained the best performance boost (3.74% and 2.68%) over the baseline of AlexNet and ConvMixer respectively.

The detail results are shown in Table 1. Our GSC loss significantly boosts the Top-1 accuracy of AlexNet, superior to focal loss, LS, and original CE loss by 1.18%, 1.44%, and 3.74%, respectively. In addition, by following the entropy formulation of Yao et al. [2020], the entropy loss can be embedded in to CE loss easily and one total loss function can be written as $L(S, Y) = CE(S, Y) + \lambda H(S)$, where λ denote the strength of the modulating term of $H(S)$. As shown in Table 1, there is a clear gap between the best accuracy of entropy loss and our GSC loss (2.86%).

Model	Loss FUN	Parameters	Top-1%	Top-5%
AlexNet	CE loss	-	73.33	98.01
AlexNet	+Entropy	0.02;-	74.21(0.88 \uparrow)	98.02
AlexNet	Focal loss	2;-	75.10(1.77 \uparrow)	98.38
AlexNet	+LS	0.1;-	76.31(2.98 \uparrow)	98.09
AlexNet	+GSC	0.05,2	77.07(3.74 \uparrow)	98.00
AlexNet	Focal loss	2;-	75.10	98.38
AlexNet	+GSC	2;0.02,3	76.28(1.18 \uparrow)	98.14
AlexNet	CE + LS	0.1;-	76.31	98.09
AlexNet	+GSC	0.1;0.03,2	77.75(1.44 \uparrow)	97.60
ConvMixer	CE loss	-	89.79	99.70
ConvMixer	+GSC	0.02,3	92.47(2.68 \uparrow)	99.78

Table 1: Recognition accuracy of different methods on CIFAR10. The parameters ($\lambda, \eta, \alpha, \gamma$ and top_c) are for entropy loss, focal loss, LS and GSC loss, respectively.

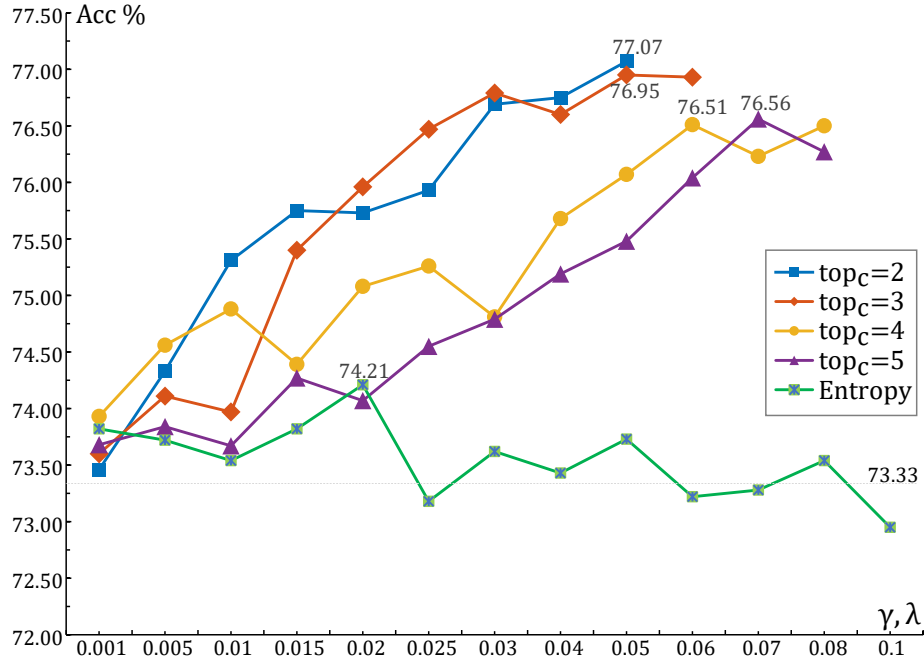


Figure 5: The classification performance of GSC loss and entropy loss, when varying γ, λ for GSC loss (w. optimal top_c) and the entropy loss.

Effectiveness of λ, γ and top_c on CIFAR-10: Two parameters (γ and top_c) were introduced to control the strength and dimension of the proposed GSC loss respectively. The relation between the accuracy and parameter γ with different top_c on CIFAR-10 was reported in Fig. 5. With the increase of γ and a fixed top_c , one can note that the accuracy of our GSC loss will be on the rise. With $top_c = 3$ or 5, the accuracy- γ curves (the purple and red line) are smoother i.e., the flutter range of them are smaller. In contrast, with $top_c = 2$ or 4, the curves (the blue and yellow line) are sharp i.e., the flutter range of them are larger. The best performance was obtained with $top_c = 2$ and the fixed γ . Therefore, all experiments with GSC loss will start with the $\gamma = 0.01$ and $top_c = 2$ or 3. Notably, the performance of those parameter settings all outperform the baseline 73.33% (the gray dotted line) by at least 0.13%. To facilitate comparison of GSC and entropy loss, the effectiveness of parameter λ (the green one) for entropy loss was also drawn in Fig. 5. Although the entropy loss is superior to original CE loss by a small margin (0.88%), the accuracy- λ curve is jittering up and down around the baseline.

Tolerance to Noisy Labels on CIFAR-10: To verify the regularization capability of our GSC loss on noisy data, the experiments with the same settings as Wang et al. [2019] on CIFAR-10 were conducted. According to the noise rate, a certain number of samples are randomly selected and flipped to the wrong labels before training. The top-1 recognition

Method	γ, top_c	NR=20%	NR=40%	NR=60%	NR=80%
CE loss	-	72.51	68.95	63.45	43.38
+GSC	2.0,5	74.89	70.22	62.17	42.17
+GSC	0.8,3	74.81	70.53	62.32	39.31
+GSC	0.2,2	74.24	70.49	63.65	42.53
+GSC	0.05,2	74.02	69.82	63.38	43.83

Table 2: Under four noise rates (NR), the top-1 recognition accuracy with CE and GSC loss on CIFAR-10.

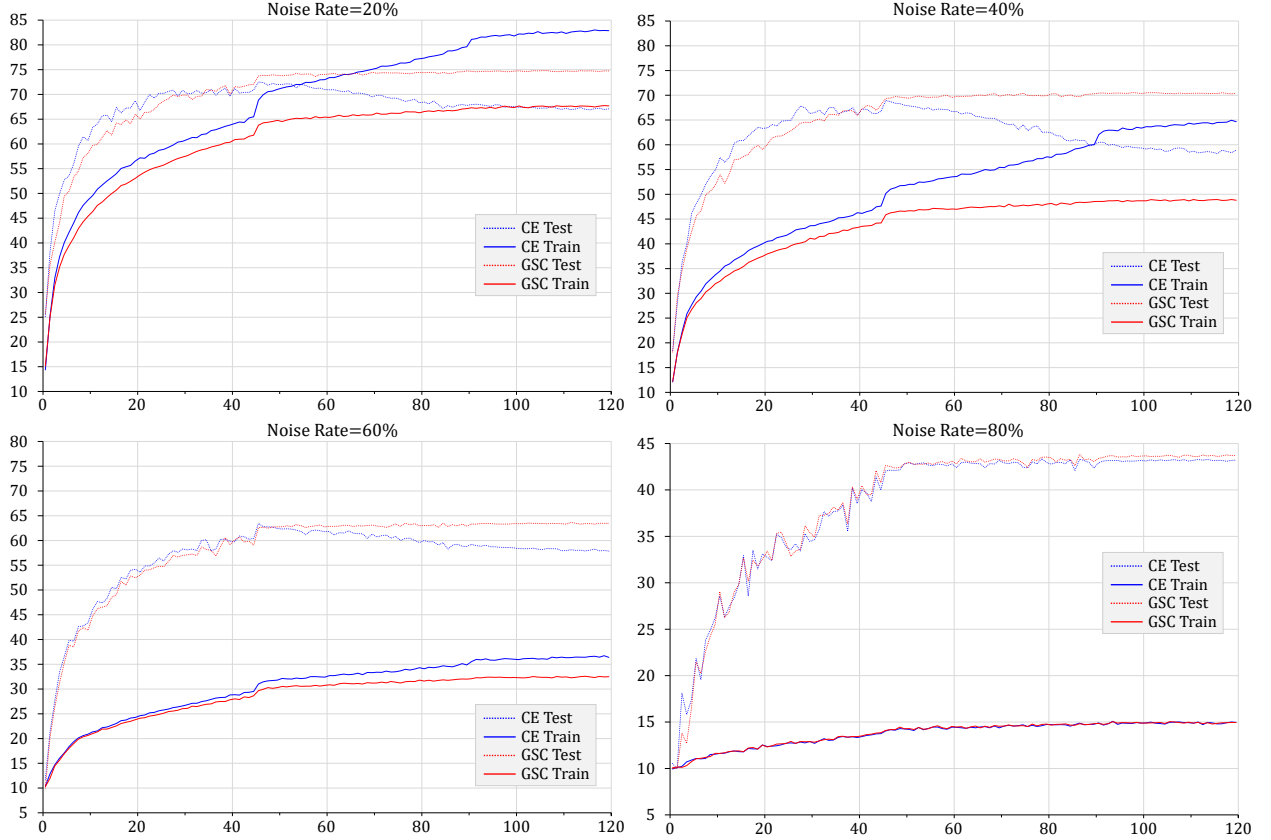


Figure 6: Under four noise rates, the training and test accuracy vs. iteration on CIFAR-10.

accuracy results under four noisy rates (20%, 40%, 60%, 80%) were reported in Table 2. Compared to the CE loss, the stable improvements under different noisy rates were obtained by our GSC loss.

In addition, the training and test accuracy vs. iteration was visualized in Fig. 6. We note that the training and the test accuracy curves of CE loss are intersected during the training process with the 20% and 40% noise rates, and the training accuracy exceed 80% and 60% respectively, which are typical overfitting phenomenons. By contrast, the proposed GSC loss not only enables the model to be trained normally, but also achieves better classification performance. However, when the noise rate is high (80%), the performance of CE loss is similar to our GSC loss.

ImageNet-1K: We employ the settings of ResNet-50/101 in Radosavovic et al. [2020]. ImageNet-1K (1K-class) consists of $\sim 1.28M$ images for training and 50K validation images. We conduct experiments by utilizing the same comparison protocols and data augmentation as Radosavovic et al. [2020]. The detailed results are reported in Table 3. When $\gamma = 0.02, top_c = 7$, GSC loss is superior to the baseline of ResNet-50 by 0.54%. Especially when $\gamma = 0.02, top_c = 5$, GSC loss can further reduce the error rate of ResNet101 baseline from 21.26% to 20.79%. The error rates of most related methods, including LS, Online Label Smoothing (OLS) strategy, and CutOut DeVries and Taylor [2017] which are reported in Zhang et al. [2021], are shown in Table 3. The comparison result demonstrates that our GSC loss performs favorably against SOTA methods with training only 100 epochs.

Model	Method	Avg. Top-1%	Avg. Top-5%	Epochs
RN-50	CE loss	23.68†	7.05†	250
RN-50	LS	22.82†	6.66†	250
RN-50	CutOut	22.93†	6.66†	250
RN-50	OLS	22.28†	6.39†	250
RN-101	CE loss	21.87†	6.29†	250
RN-101	LS	21.27†	5.85†	250
RN-101	CutOut	20.72†	5.51†	250
RN-101	OLS	20.85†	5.50†	250
RN-50	CE loss	23.03($\pm 1.24e-03$)	6.55($\pm 7.69e-04$)	100
RN-50	+GSC	22.49 ($\pm 2.25e-04$)	6.35 ($\pm 4.00e-06$)	100
RN-101	CE loss	21.26($\pm 2.10e-03$)	5.66($\pm 6.93e-05$)	100
RN-101	+GSC	20.79 ($\pm 1.43e-03$)	5.46 ($\pm 1.49e-04$)	100

Table 3: Recognition error rate on ImageNet-1K classification benchmark. †denotes the results reported in Zhang et al. [2021]. ResNet is abbreviated as RN.

Method	γ, top_c	Top-1 %	Top-5 %
CE loss	-	90.69†	97.57†
+GSC	0.05,9	92.36 (1.67 ↑)	98.10
CE+LS	-	92.42†	98.07†
+GSC	0.05,3	93.12 (0.70 ↑)	98.28
CE+OLS	-	92.86†	98.45†
+GSC	0.005,11	93.49 (0.63 ↑)	98.05

Table 4: Recognition accuracy on Flowers-102 dataset with the architecture of ResNet-50. †denotes the results reported in Zhang et al. [2021].

Flowers-102: We employ the settings of ResNet-50 in Zhang et al. [2021]. Unlike general classification tasks, fine-grained classification focuses on the sub-category level. To demonstrate the effectiveness of our method for classification tasks of different granularity, we conducted experiments on Flowers-102 and the results are shown in Table 4. Experimental results note that our GSC loss is effective in fine-grained classification and also achieves significant improvement based on LS and OLS.

4.2 Face Verification

We follow the same experiments settings as Arcface. The GSC loss was introduced into the network of face verification to enhance the baseline performance. To compare with state-of-the-art face verification methods, the advanced methods including PSN Srivastava et al. [2019], (R+D)BM Cao et al. [2020] and FAPS_C Xu et al. [2021] are introduced in Table

Method	γ, top_c	LFW %	CALFW %	CFP-FF %	γ, top_c	CPLFW %	CFP-FP %	AgeDB-30 %
RBM	-	99.10‡	91.00‡	-	-	87.10‡	-	91.30‡
DBM	-	99.20‡	92.00‡	-	-	87.30‡	-	91.90‡
R&D	-	99.30‡	92.50‡	-	-	87.60‡	-	92.10‡
Arcface	-	99.10*	89.05*	-	-	78.43*	-	93.18*
FAPS _C	-	99.20*	89.47*	-	-	80.28*	-	94.02*
Cosface	-	99.100	93.033	99.429	-	86.783	92.871	93.167
+GSC	0.015,3	99.217(0.117 ↑)	93.267(0.234 ↑)	99.300	0.05,5	87.350(0.570 ↑)	92.914(0.043 ↑)	93.750(0.583 ↑)
+GSC	0.025,3	99.233(0.133 ↑)	93.117(0.084 ↑)	99.529(0.100 ↑)	0.01,2	87.400(0.617 ↑)	93.057(0.186 ↑)	93.350(0.183 ↑)
+GSC	0.025,2	99.300(0.200 ↑)	92.850	99.371	0.02,2	87.483(0.700 ↑)	93.000(0.129 ↑)	93.450(0.283 ↑)
Arcface	-	99.200	93.300	99.414	-	86.833	93.343	93.267
+GSC	0.01,3	99.283(0.083 ↑)	93.417(0.117 ↑)	99.471(0.057 ↑)	0.025,3	86.550	93.557(0.214 ↑)	93.700(0.433 ↑)
+GSC	0.03,5	99.250(0.050 ↑)	93.350(0.050 ↑)	99.529(0.115 ↑)	0.02,3	86.683	93.443(0.100 ↑)	93.950(0.683 ↑)
+GSC	0.015,2	99.217(0.017 ↑)	93.383(0.083 ↑)	99.257	0.02,2	87.050(0.217 ↑)	93.486(0.143 ↑)	93.717(0.450 ↑)

Table 5: Verification performance of different methods on LFW, CALFW, CFP-FF, CPLFW, CFP-FP and AgeDB-30.

Loss FUN	γ, top_c	Test %	Validation %
CE loss	-	72.12	73.82
+GSC	0.01,2	72.72(0.60 \uparrow)	73.25
+GSC	0.015,2	72.17(0.05 \uparrow)	74.39(0.57 \uparrow)
+GSC	0.01,3	72.39(0.27 \uparrow)	74.17(0.35 \uparrow)
+GSC	0.02,3	72.25(0.13 \uparrow)	74.37(0.55 \uparrow)

Table 6: Recognition accuracy of test and validation data on FER2013 dataset.

5 (\dagger , \ddagger and $*$ denote the results reported in Srivastava et al. [2019], Cao et al. [2020], Xu et al. [2021], respectively). The performance of GSC loss embedded into Arcface and Cosface is superior to all other methods in LFW, CALFW and CFP-FF/FP, indicating the proposed GSC loss is a benefit for achieving a SOTA result for the face verification tasks.

Results on LFW, CALFW, CFP-FF, CPLFW, CFP-FP and AgeDb-30: Table 5 presents the results of GSC loss on those datasets. For LFW, with all γ, top_c settings, GSC loss can boost the accuracy, attaining 0.017%-0.200% improvement over the baseline of Arcface and Cosface, respectively. When $\gamma = 0.01, top_c = 3$ and $\gamma = 0.015, top_c = 3$, GSC loss can obviously boost the performance over the baseline of Arcface and Cosface on CALFW (0.117% and 0.234% respectively, which are significant accuracy increases). Moreover, with $\gamma = 0.03, top_c = 5$, GSC loss can further improve the accuracy baseline of Arcface from 99.414% to 99.529%. GSC loss also improves the accuracy baseline of Cosface from 99.429% to 99.529% while $\gamma = 0.025, top_c = 3$. For CFP-FP, GSC loss can boost the accuracy, attaining 0.043%-0.214% improvement over the baseline of Arcface and Cosface respectively with all γ, top_c settings. As $\gamma = 0.02, top_c = 3$ and $\gamma = 0.02, top_c = 2$, GSC loss can outperform the baseline of Arcface and Cosface by obvious margins (0.683% on AgeDb-30 and 0.700% on CPLFW respectively, which are notable improvements). Moreover, on AgeDb-30 and CFP-FP, our GSC loss can widely improve the baseline performance of Arcface and Cosface.

4.3 Facial Emotion Recognition

We follow the experiment settings of the modified VGGNet Khairuddin and Chen [2021]. The long-tailed FER2013 dataset contains $\sim 36K$ images consisting of 7 different emotions consisting of anger, neutral, disgust, fear, happiness, sadness, and surprise. A Kaggle forum discussion places human accuracy on this dataset in the range of 65–68%. For training and evaluation, we employ the official train, validation, and test protocols as introduced by Goodfellow et al. [2013b].

The detailed results of GSC and CE loss are reported in Table 6. We note that GSC loss is superior to both the baselines of the test set and validation set by 0.6% and 0.57%, respectively. In particular, when $top_c = 2$, slightly varies γ from 0.01 to 0.015, the best performances are obtained in the validation set and test set, respectively. Although the best accuracy of 72.72% is obtained in the test set, the accuracy of the validation set is inferior to the baseline. According to our analysis, the data distributions of test and validation sets may be notably different. When $top_c = 3$, slightly varying γ from 0.01 to 0.02, considerable balanced performances can be achieved on both test and validation sets.

As shown in Fig. 7(a), the loss in the training set continues to decline, but the loss in the validation set is increasing, which is a typical overfitting phenomenon. Despite the loss of the validation set continuously rising, the accuracy of the validation set is also increasing. In our option, to further reduce the training loss, the CE loss mainly focuses on fitting well-classified samples. That is, the score of class label $y = 1$ in the validation set is reduced but still gives the correct prediction results. In contrast, our GSC loss in training and validation set all continue to decline until hold stable. Notably, the training loss of the proposed GSC loss is larger than the CE loss, but the validation accuracy is greater than the CE loss. It demonstrates GSC loss mainly focuses on fitting the poor-classified samples and can alleviate overfitting.

4.4 Unsupervised Image Segmentation

As introduced before, our GSC loss could be applied to several unsupervised learning tasks. Herein, we conduct an exploration namely unsupervised image segmentation by following a pioneer work Kanezaki [2018]. For this task, γ is chosen from $[0.1, 0.5]$ and top_c is set as $\{7, 9\}$. Fig. 8 presents the qualitative comparison between the ground truth, baseline, and our GSC loss. Both in the woof (first row) and waterfowl (second row) picture, more precise segments with various colors and textures are detected by our GSC loss. More specifically, GSC groups pixels within woof and waterfowl objects into a single category compared to baseline.

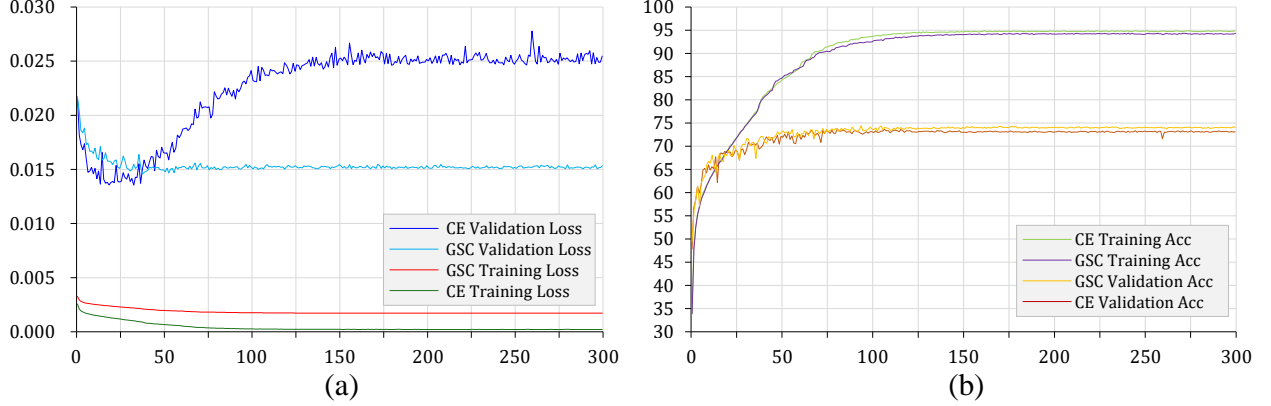


Figure 7: Loss value and accuracy vs. iteration with GSC and CE loss. As training progresses, the GSC validation loss goes down consistently, see the light blue curve in (a). The variance across iterations is smaller than that of the CE validation loss, see the blue curve in (a).

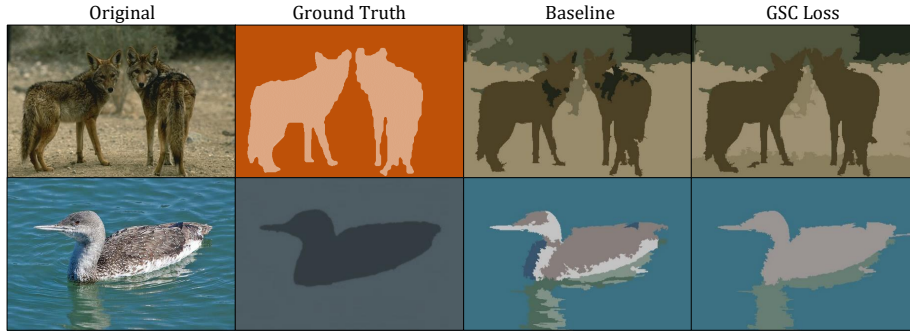


Figure 8: Qualitative results of the baseline and ours for unsupervised image segmentation. The original images are in the first column, the second consists of the ground truth images, the next contains the results of the baseline, and our segmentation results are in the last column. Different segments are shown in different colors.

5 Conclusion

Inspired by the derivative of the entropy function, we formulate GSC loss from a novel perspective of the distribution of predicted scores from the softmax layer to enhance the performance of CE loss, and a clear theoretical basis and explanation were given. Notably, the plug-and-play GSC loss does not rely on labels and increases model parameters. We demonstrated its efficacy by conducting 5 classification visual tasks over 10 benchmark datasets. Moreover, the profits from GSC loss are complementary to such CE based methods as Arcface, focal loss, LS and OLS. We further demonstrate that GSC loss can yield obvious improvements for the unsupervised image segmentation. The code will be released soon.

6 Appendix

6.1 Action Recognition on NTU RGB+D

We employ the same experiment settings of ResNet3D-34 Ji et al. [2021]. All experiments employ the SGD optimizer with fixed momentum of 0.9 and weight decay of 10^{-5} . We set the LR at 0.01, and it decreases to one-tenth times every 20 epochs.

NTU RGB+D consists of 60 classes, a large multi-modal dataset, contains 56880 action sequences captured with three cameras from different views. We follow the cross-subject (X-Sub) and cross-view (X-View) protocols introduced by Shahroudy et al. [2016] to conduct all experiments. Table 7 reports comparison results, for the cross-subject, with $\gamma = 0.02$, $top_c = 3$, GSC loss yields an obvious improvement over the CE loss (0.69%). As $\gamma = 0.02$, $top_c = 2$, our

Loss FUN	γ, top_c	X-Sub %	X-View %
CE loss	-	87.87	90.82
+GSC	0.02,3	88.56(0.69 \uparrow)	-
+GSC	0.02,2	-	91.37(0.55 \uparrow)

Table 7: Recognition accuracy (%) of cross-subject and cross-setup evaluations on NTU RGB+D.

GSC loss achieves a noteworthy increase over the CE loss in the protocol of cross-view (0.55%). One can note that proposed GSC loss can yield consistent boosts in Spatio-Temporal modeling networks.

6.2 Backward Gradient of GSC Loss

(p_1^i, p_2^i)	$H(p^i)$	$H'(p^i)$	$f(p^i)$	$f'(p^i)$
(0.50 , 0.50)	0.693	0.000	0.197	0.205
(0.55 , 0.45)	0.688	0.201	0.197	0.187
(0.60 , 0.40)	0.673	0.405	0.198	0.175
(0.65 , 0.35)	0.647	0.619	0.198	0.165
(0.70 , 0.30)	0.611	0.847	0.196	0.158
(0.75 , 0.25)	0.562	1.099	0.187	0.148
(0.80 , 0.20)	0.500	1.386	0.163	0.131
(0.85 , 0.15)	0.423	1.735	0.111	0.093
(0.90 , 0.10)	0.325	2.197	0.031	0.029

Table 8: Comparison of $H(p^i)$, $H'(p^i)$, $f(p^i)$ and $f'(p^i)$ function values.

It is straightforward to compute the forward and backward propagation for proposed GSC loss. It is also easy to optimize the GSC loss with an SGD optimizer. We infer the gradient descent of GSC loss for binary classification and discover that when the predicted scores become similar, the gradient value of our GSC loss persists. We start with the derivative of p for $f_2(p, \sigma_i)$, see Eq. 17 for the explicit derivation process.

$$\frac{\partial f_2(p, \sigma_i)}{\partial p} = f_2(p, \sigma_i) \frac{1-p}{\sigma_i^2}. \quad (12)$$

To simplify the calculation, we assume that σ_i is a constant and $f_2(p, \sigma_i)$ can be abbreviated as $f(p)$. We let $p_1^i = p$ denotes the score of class label $y = 1$, $p_2^i = 1 - p$ denotes $y = 0$. Then substitute p^i into Eq. 15 and 12, and compute $H(p^i)$, $H'(p^i)$, $f(p^i)$ and $f'(p^i)$ respectively. The results are shown in Table 8. As p increases from 0.5 to 0.9, the value of entropy function $H(p)$ decreases from 0.693 to 0.325 and our GSC $f(p)$ decreases from 0.197 to 0.031. Notably, the absolute value of $H'(p)$ rapidly increases from 0 to 2.197, while the gradient of our $f(p)$ faintly decreases from 0.205 to 0.029. The initial output scores usually obey a uniform distribution, the model needs larger backward gradient to enhance the confidence of prediction. Later in training, some models produce an over-confidence score, the confidence of model should not be strengthened.

6.3 Experiment Settings of Face Verification

For model training, we employ the commonly used web-collected outside dataset CASIA Yi et al. [2014] (excluding the images of identities appearing in the test set) which has $\sim 0.5M$ face images belonging to $\sim 10K$ different individuals.

For the validation, six datasets including LFW, CALFW, CFP-FF, CPLFW, CFP-FP, and AgeDb-30 are utilized to evaluate the performance. LFW includes $\sim 13K$ web-collected images from $\sim 5K$ different identities, with limited variations in pose, age, expression, and illuminations. CPLFW was collected from LFW with a larger pose gap. Similar to CPLFW, CALFW was selected from LFW with higher variations of age. CFP consists of collected images of celebrities in frontal and profile views, which has two evaluation protocols consisting of CFP-Frontal-Frontal and CFP-Frontal-Profile which is a more challenging protocol with around a 90° pose gap within positive pairs. AgeDB-30, a ‘‘in-the-wild’’ dataset, contains manually annotated images. In this paper, we employ the evaluation protocol with a 30-year gap. Table 9 lists the details of these datasets.

Datasets	#Identity	#Image
LFWHuang et al. [2008]	5749	13233
CASIA Yi et al. [2014]	10K	0.5M
CFP-FP/FFSengupta et al. [2016]	500	7000
AgeDB-30Moschoglou et al. [2017]	568	16488
CALFWZheng et al. [2017]	5749	12174
CPLFWZheng and Deng [2018]	5749	11652

Table 9: Face datasets for training and validation.

6.4 Some Details About Formulas

For binary classification, we define $S_1 = p$ and $S_2 = 1 - p$. Then GSC loss can be formulated as

$$\mathbf{f}_2(S, \boldsymbol{\mu}, \boldsymbol{\sigma}) = \frac{1}{2\pi\sigma_i^2} \exp\left[-\frac{(2p^2 - 2p + 1)}{2\sigma_i^2}\right]. \quad (13)$$

Thus, the final loss function for binary classification is defined as

$$L(S, Y) = CE(S, Y) + \gamma \mathbf{f}_2(S, \boldsymbol{\mu}, \boldsymbol{\sigma}), \quad (14)$$

where $\mu_i = 0, \sigma_i = E(S)$ and $\gamma \geq 0$ is a hyper-parameter.

Derivative of p for $H(p)$,

$$\begin{aligned} H'(p) &= -[p \log(p) + (1-p) \log(1-p)]' \\ &= -[\log(p) - \log(1-p)] \\ &= \log\left(\frac{1-p}{p}\right). \end{aligned} \quad (15)$$

Derivative of p for $\mathbf{f}_2(p, \sigma_i)$, Let:

$$\begin{cases} m(\sigma_i) = \frac{1}{2\pi\sigma_i^2} \exp\left[-\frac{1}{2\sigma_i^2}\right], \\ n(p, \sigma_i) = \frac{(2p - 2p^2)}{2\sigma_i^2}. \end{cases} \quad (16)$$

Then, substituting Eq. 16 into Eq. 13.

$$\begin{aligned} \frac{\partial \mathbf{f}_2(p, \sigma_i)}{\partial p} &= m(\sigma_i) \exp[n(p, \sigma_i)]' \\ &= m(\sigma_i) \exp[n(p, \sigma_i)] n(p, \sigma_i)' \\ &= \mathbf{f}_2(p, \sigma_i) \frac{1-p}{\sigma_i^2}. \end{aligned} \quad (17)$$

As discussed in the section 1, our GSC loss can be easily embedded into the recent improved methods of CE loss. The total loss function consist of focal loss and GSC loss can be written as

$$L(S, Y) = (1 - SY)^\eta CE(S, Y) + \gamma \mathbf{f}_{top_c}(S', H(S)), \quad (18)$$

where η denotes the strength of the modulating term of focal loss.

References

- Geoffrey E Hinton, Nitish Srivastava, Alex Krizhevsky, Ilya Sutskever, and Ruslan R Salakhutdinov. Improving neural networks by preventing co-adaptation of feature detectors. *arXiv preprint arXiv:1207.0580*, 2012.
- Ian Goodfellow, David Warde-Farley, Mehdi Mirza, Aaron Courville, and Yoshua Bengio. Maxout networks. In *International conference on machine learning*, pages 1319–1327. PMLR, 2013a.
- Christian Szegedy, Vincent Vanhoucke, Sergey Ioffe, Jon Shlens, and Zbigniew Wojna. Rethinking the inception architecture for computer vision. In *Proceedings of the IEEE conference on computer vision and pattern recognition*, pages 2818–2826, 2016.

- Barret Zoph, Vijay Vasudevan, Jonathon Shlens, and Quoc V Le. Learning transferable architectures for scalable image recognition. In *Proceedings of the IEEE conference on computer vision and pattern recognition*, pages 8697–8710, 2018.
- Chang-Bin Zhang, Peng-Tao Jiang, Qibin Hou, Yunchao Wei, Qi Han, Zhen Li, and Ming-Ming Cheng. Delving deep into label smoothing. *IEEE Transactions on Image Processing*, 30:5984–5996, 2021.
- Chuan Guo, Geoff Pleiss, Yu Sun, and Kilian Q Weinberger. On calibration of modern neural networks. In *International Conference on Machine Learning*, pages 1321–1330. PMLR, 2017.
- Jiankang Deng, Jia Guo, Niannan Xue, and Stefanos Zafeiriou. Arcface: Additive angular margin loss for deep face recognition. In *Proceedings of the IEEE/CVF Conference on Computer Vision and Pattern Recognition*, pages 4690–4699, 2019.
- Raia Hadsell, Sumit Chopra, and Yann LeCun. Dimensionality reduction by learning an invariant mapping. In *2006 IEEE Computer Society Conference on Computer Vision and Pattern Recognition (CVPR’06)*, volume 2, pages 1735–1742. IEEE, 2006.
- Florian Schroff, Dmitry Kalenichenko, and James Philbin. Facenet: A unified embedding for face recognition and clustering. In *Proceedings of the IEEE conference on computer vision and pattern recognition*, pages 815–823, 2015.
- Weiyang Liu, Yandong Wen, Zhiding Yu, and Meng Yang. Large-margin softmax loss for convolutional neural networks. In *ICML*, volume 2, page 7, 2016.
- Weiyang Liu, Yandong Wen, Zhiding Yu, Ming Li, Bhiksha Raj, and Le Song. Sphereface: Deep hypersphere embedding for face recognition. In *Proceedings of the IEEE conference on computer vision and pattern recognition*, pages 212–220, 2017.
- Hao Wang, Yitong Wang, Zheng Zhou, Xing Ji, Dihong Gong, Jingchao Zhou, Zhifeng Li, and Wei Liu. Cosface: Large margin cosine loss for deep face recognition. In *Proceedings of the IEEE conference on computer vision and pattern recognition*, pages 5265–5274, 2018.
- Rafael Müller, Simon Kornblith, and Geoffrey Hinton. When does label smoothing help? *arXiv preprint arXiv:1906.02629*, 2019.
- Yichun Shi and Anil K. Jain. Probabilistic face embeddings. In *Proceedings of the IEEE/CVF International Conference on Computer Vision (ICCV)*, October 2019.
- Abhinav Shrivastava, Abhinav Gupta, and Ross Girshick. Training region-based object detectors with online hard example mining. In *Proceedings of the IEEE conference on computer vision and pattern recognition*, pages 761–769, 2016.
- Kamal Nigam, John Lafferty, and Andrew McCallum. Using maximum entropy for text classification. In *IJCAI-99 workshop on machine learning for information filtering*, volume 1, pages 61–67. Stockholm, Sweden, 1999.
- Tsung-Yi Lin, Priya Goyal, Ross Girshick, Kaiming He, and Piotr Dollár. Focal loss for dense object detection. In *Proceedings of the IEEE international conference on computer vision*, pages 2980–2988, 2017.
- James V Zidek and Constance van Eeden. Uncertainty, entropy, variance and the effect of partial information. *Lecture Notes-Monograph Series*, pages 155–167, 2003.
- Kaiming He, Xiangyu Zhang, Shaoqing Ren, and Jian Sun. Deep residual learning for image recognition. In *CVPR*, pages 770–778, 2016.
- Maria-Elena Nilsback and Andrew Zisserman. Automated flower classification over a large number of classes. In *2008 Sixth Indian Conference on Computer Vision, Graphics & Image Processing*, pages 722–729. IEEE, 2008.
- Alex Krizhevsky. One weird trick for parallelizing convolutional neural networks. *arXiv preprint arXiv:1404.5997*, 2014.
- Asher Trockman and J Zico Kolter. Patches are all you need? *arXiv preprint arXiv:2201.09792*, 2022.
- Chen-Yu Lee, Saining Xie, Patrick Gallagher, Zhengyou Zhang, and Zhuowen Tu. Deeply-supervised nets. In *Artificial intelligence and statistics*, pages 562–570. PMLR, 2015.
- Yao Yao, Jiehui Deng, Xiuhua Chen, Chen Gong, Jianxin Wu, and Jian Yang. Deep discriminative cnn with temporal ensembling for ambiguously-labeled image classification. In *Proceedings of the AAAI Conference on Artificial Intelligence*, volume 34, pages 12669–12676, 2020.
- Yisen Wang, Xingjun Ma, Zaiyi Chen, Yuan Luo, Jinfeng Yi, and James Bailey. Symmetric cross entropy for robust learning with noisy labels. In *Proceedings of the IEEE/CVF International Conference on Computer Vision*, pages 322–330, 2019.

- Ilija Radosavovic, Raj Prateek Kosaraju, Ross Girshick, Kaiming He, and Piotr Dollár. Designing network design spaces. In *CVPR*, 2020.
- Terrance DeVries and Graham W Taylor. Improved regularization of convolutional neural networks with cutout. *arXiv preprint arXiv:1708.04552*, 2017.
- Yash Srivastava, Vaishnav Murali, and Shiv Ram Dubey. Psnet: Parametric sigmoid norm based cnn for face recognition. In *2019 IEEE Conference on Information and Communication Technology*, pages 1–4. IEEE, 2019.
- Dong Cao, Xiangyu Zhu, Xingyu Huang, Jianzhu Guo, and Zhen Lei. Domain balancing: Face recognition on long-tailed domains. In *Proceedings of the IEEE/CVF Conference on Computer Vision and Pattern Recognition*, pages 5671–5679, 2020.
- Xiaqing Xu, Qiang Meng, Yunxiao Qin, Jianzhu Guo, Chenxu Zhao, Feng Zhou, and Zhen Lei. Searching for alignment in face recognition. In *Proceedings of the AAAI Conference on Artificial Intelligence*, volume 35, pages 3065–3073, 2021.
- Yousif Khairuddin and Zhuofa Chen. Facial emotion recognition: State of the art performance on fer2013. *arXiv preprint arXiv:2105.03588*, 2021.
- Ian J Goodfellow, Dumitru Erhan, Pierre Luc Carrier, Aaron Courville, Mehdi Mirza, Ben Hamner, Will Cukierski, Yichuan Tang, David Thaler, Dong-Hyun Lee, et al. Challenges in representation learning: A report on three machine learning contests. In *International conference on neural information processing*, pages 117–124. Springer, 2013b.
- Asako Kanezaki. Unsupervised image segmentation by backpropagation. In *2018 IEEE international conference on acoustics, speech and signal processing (ICASSP)*, pages 1543–1547. IEEE, 2018.
- Xiaopeng Ji, Qingsong Zhao, Jun Cheng, and Chenfei Ma. Exploiting spatio-temporal representation for 3d human action recognition from depth map sequences. *Knowledge-Based Systems*, page 107040, 2021.
- Amir Shahroudy, Jun Liu, Tian-Tsong Ng, and Gang Wang. Ntu rgb+ d: A large scale dataset for 3d human activity analysis. In *CVPR*, pages 1010–1019, 2016.
- Dong Yi, Zhen Lei, Shengcai Liao, and Stan Z Li. Learning face representation from scratch. *arXiv preprint arXiv:1411.7923*, 2014.
- Gary B Huang, Marwan Mattar, Tamara Berg, and Eric Learned-Miller. Labeled faces in the wild: A database for studying face recognition in unconstrained environments. In *Workshop on faces in 'Real-Life' Images: detection, alignment, and recognition*, 2008.
- Soumyadip Sengupta, Jun-Cheng Chen, Carlos Castillo, Vishal M Patel, Rama Chellappa, and David W Jacobs. Frontal to profile face verification in the wild. In *2016 IEEE Winter Conference on Applications of Computer Vision (WACV)*, pages 1–9. IEEE, 2016.
- Stylianos Moschoglou, Athanasios Papaioannou, Christos Sagonas, Jiankang Deng, Irene Kotsia, and Stefanos Zafeiriou. Agedb: the first manually collected, in-the-wild age database. In *Proceedings of the IEEE Conference on Computer Vision and Pattern Recognition Workshops*, pages 51–59, 2017.
- Tianyue Zheng, Weihong Deng, and Jiani Hu. Cross-age lfw: A database for studying cross-age face recognition in unconstrained environments. *arXiv preprint arXiv:1708.08197*, 2017.
- Tianyue Zheng and Weihong Deng. Cross-pose lfw: A database for studying cross-pose face recognition in unconstrained environments. *Beijing University of Posts and Telecommunications, Tech. Rep*, 5:7, 2018.